A Pendulum-Driven Legless Rolling Jumping Robot

Jake Buzhardt[1], Prashanth Chivkula[1] and Phanindra Tallapragada[1]

***Abstract*— In this paper, we present a novel rolling, jumping robot. The robot consists of a driven pendulum mounted to a wheel in a compact, lightweight, 3D printed design. We show that by using the driven pendulum to change it's weight distribution, the robot is able to obtain significant rolling speed, achieve jumps of up to 2.5 body lengths vertically, and also clear horizontal distances of over 6 body lengths while jumping. The robot's dynamic model is derived and simulation results indicate that it is consistent with the motion and jumping observed on the robot. The ability to both roll and jump effectively using a minimalistic design makes this robot unique and could inspire the use of similar mechanisms on robots intended for applications in which agile locomotion on unstructured terrain is necessary, such as disaster response or planetary exploration.**

I. Introduction

The mobility of a robot in unstructured terrain can greatly improve with the ability to execute small hops or jumps repeatedly with little relaxation. Even robots which operate in structured environments can benefit from an ability to hop on small steps or jump over obstacles. Several designs of robots have sought to incorporate a jumping or hopping gait into the repertoire of a robot's gaits. A common feature of most designs that produce jumping is a mechanism to store potential energy that can be released in a short interval. The resulting conversion of the potential energy to kinetic energy in the vertical direction leads to a jump. The most popular method to achieve such storage and release of energy is via traditional elastic elements, such as compression of torsional springs or flexural plates and columns. Some well known examples that adopt such design include the MSU jumper [1], the Penn Jerboa [2], the Grillo [3] and the Salto [4] and other impressive bioinspired micro jumping robots [5].

This paper revisits the theoretical concept of a jump as a discontinuity in holonomic constraints and advances the idea that purely internal shape variables without an elastic element can produce such a discontinuity. This design is inspired by the complex dynamics of a rolling hoop with an unbalanced mass, the so-called Littlewood hoop [6], which has been the subject of many theoretical and experimental investigations [7]–[11]. Just as the original works on passive walking [12], [13] inspired the development of many actuated walking mechanisms [14], here we let the passive rolling jumping mechanism of Littlewood's hopping hoop serve as inspiration for an actuated rolling, jumping robot. The specific design we use in this paper is a cylinder that contains an actuated internal pendulum. This wheel mechanism can roll due to a torque exerted via the internal pendulum and a high speed swing of the pendulum produces a discontinuity in the normal reaction on the robot from the ground leading to a jump. With such a framework, even in the first design iteration, the robot is capable of a vertical jump height of over two body lengths and a horizontal jump distance of over 6 body lengths. Furthermore the robot can execute repeated jumps without a long relaxation time. The repeated jumping motion takes advantage of the slip motion of the cylinder upon impact and the resulting friction force.

The proposed legless rolling-jumping robot is distinct in design and mechanics from the existing few jumping robots that can also roll or tip over repeatedly. Past rolling-jumping robots such as [15]–[17] still relied on elastic components or shape memory to store and release energy. For instance the jollbot in [15] is an elastic spheroid which uses a pendulum mechanism for rolling, but can also compress and change shape significantly to store elastic potential energy that can be released for a jump of about 0.6 body lengths. The two wheeled robot in [17] has an elastic chassis that can snap through and buckle and produce a jump that is 0.25 body lengths in height and 1 body lengths in width. Despite the lack of any elastic components, the novel legless rolling-jumping robot presented in this paper can jump significantly higher and farther.

Another class of related robots are those which employ momentum-based strategies for rolling, walking, or jumping. For example, the robot in [18] is able to jump up and down stairs by swinging a pair of pendulum arms. Several other works have recently proposed mechanisms which utilize the transfer of angular momentum that occurs from suddenly braking a rapidly spinning momentum wheel to initiate a jumping, tipping, or standing motion [19]–[23]. However, these robots are either unable to locomote aside from their jumping behavior or rely on other mechanisms for more efficient movement. Many such jumping robots do not take advantage of other efficient modes of locomotion that may be possible on different terrains. Similarly, several robots have used pendulum-based mechanisms for rolling or walking, such as pendulum-driven rolling spheres [24] and torso-actuated walking mechanisms [25]–[27], but these applications focus only on ground-based locomotion without consideration of how such a mechanism could be used for jumping. In this paper we propose a legless robot design that is capable of two modes of motion - rolling and jumping. Even more importantly this paper presents a fresh look at the theoretical models and mechanics that can lead to the design of robots with superior mobility.

*This work was not supported by any organization

[1]The authors are with the Department of Mechanical Engineering, Clemson University, Clemson, SC, USA, {jbuzhar,pchivku,ptallap}@clemson.edu

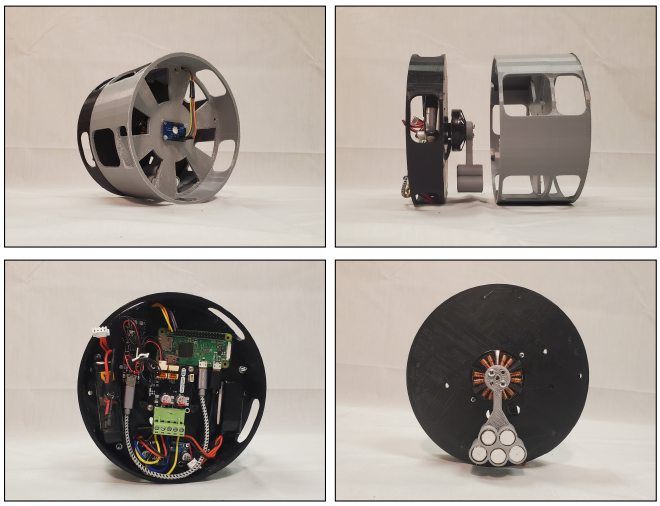

Fig. 1: Top left: pendulum-driven jumping wheel robot. Top right: side view of disassembled robot. Bottom right: Front view of pendulum mounted to a brushless DC motor affixed to the back hoop. Bottom left: rear view of robot showing electronics components

II. Robot Design and System Description

The jumping mechanism in consideration here requires a wheel body with an approximately uniform weight distribution with an offset mass attached to an arm which can be driven by a motor from the center of the wheel. Such a robot was constructed from two 3D printed hoops with a pendulum driven by a brushless DC motor affixed to the back hoop. This setup is shown in Fig. 1 and the key electronic components are summarized in Table I.

The total mass of the robot with all components attaches is approximately 600 g. The front and rear 3D printed hoops have masses of 126 g and 79 g, respectively. The total mass of the rear hoop with the motor and all electronics attached is 325 g. The pendulum consists of a 3D printed arm containing 5 steel weights inserted into cylindrical channels. Each of these pendulum weights has mass of 25 g, resulting in a total pendulum mass of 135 g and an effective offset mass of 125 g. The offset mass of the pendulum is located 51 mm from the geometric center of the hoop. The diameter of the hoop is 152 mm. The length of the two hoops together is 106mm, with the front and rear hoops having lengths 75 mm and 31 mm. These relative lengths are chosen so that the weight distribution of the robot is approximately centered along the axis passing through the centers of the hoops when the pendulum and motor are mounted to the back hoop.

TABLE I: Component specifications

Component	Specification
Motor	T-motor MN4006 KV380
Single Board Computer	Raspberry Pi Zero W
Motor Driver	Tinymovr R5
IMU	Adafruit LSM9DS0 9 DOF
CAN-USB Adapter	CANine USB-CAN adapter
Batteries	11.1 V (3S), 450 mAh
	7.4 V (2S), 400 mAh

The electronics and controls configuration of the robot consists of a T-motor MN4006 380 Kv brushless DC motor (BLDC) driven by a Tinymovr R5.1 motor driver. Being designed for use in drones, the MN4006 BLDC has a very compact and lightweight design, with a diameter of 44mm and weight of 68g, while being capable of delivering a torque of up to 0.376Nm when used with the Tinymovr R5.1. The Tinymovr driver uses field oriented control (FOC) to drive the BLDC using a built-in magnetic encoder to measure motor rotation and speed. In our application, the Tinymovr is used in velocity-control mode, in which a PI controller feeds forward a motor current value to the FOC control loop based on errors from a motor velocity reference. These control loops run at 20 kHz. The Tinymovr communicates with a Raspberry Pi Zero W over a CAN connection via the CANine CAN-USB adapter. The Raspberry Pi allows for higher level controllers to be implemented, as it delivers velocity setpoint values to the velocity control loop running on the Tinymovr. However, in this work, the velocity setpoint values are fed forward in an open-loop manner, as higher level control strategies for this robot are still the subject of ongoing work.

III. Legless Jumping - Concept and Model

The mechanical system in consideration consists of a thin hoop of mass m_o and radius R with a mass moment of inertia I_o about it's geometric center. Attached to the hoop from the center is a pendulum of mass m_p and length l_p. The arm of the pendulum is taken to be massless and the pendulum is driven relative to the hoop by a torque applied by a motor connecting the pendulum to the hoop.

We express the motion of the system in terms of the generalized coordinates $\mathbf{q} = [\phi, \theta, x, y]^T$ depicted in Fig. 2. The angles ϕ and θ denote the angles of the hoop and the pendulum, respectively, both relative to a spatially fixed frame of reference. The $\phi = \theta = 0$ configuration corresponds to the pendulum in the vertically downward position with no relative angular displacement between the pendulum and the hoop. The x and y coordinates refer to the horizontal and vertical displacement of the geometric center of the hoop, respectively, relative to a spatially fixed frame. The $y = 0$ position is defined as the configuration in which the hoop is in contact with the ground.

The kinetic energy of the system is

$$\mathcal{T} = \frac{1}{2} m_o |\mathbf{v}_o|^2 + \frac{1}{2} I_o \dot{\phi}^2 + \frac{1}{2} m_p |\mathbf{v}_p|^2 \tag{1}$$

where the velocities of the center of the hoop and the pendulum are as follows.

$$\mathbf{v}_o = \dot{x}\,\mathbf{i} + \dot{y}\,\mathbf{j} \tag{2a}$$

$$\mathbf{v}_p = \left(\dot{x} - l_p \dot{\theta} \cos\theta\right) \mathbf{i} + \left(\dot{y} + l_p \dot{\theta} \sin\theta\right) \mathbf{j}\,. \tag{2b}$$

Here, $\mathbf{i}$ and $\mathbf{j}$ are the unit vectors associated with the spatially fixed reference frame. The potential energy of the system is

$$\mathcal{V} = m_o g y + m_p g (y - l_p \cos\theta) \tag{3}$$

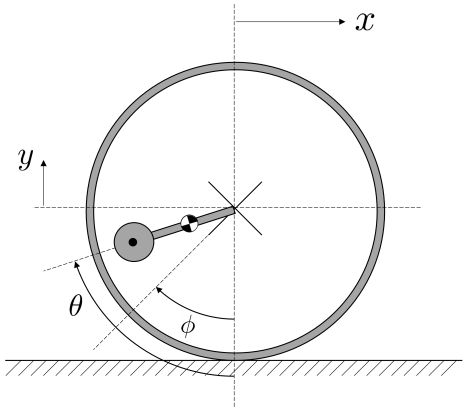

Fig. 2: Pendulum-driven wheel robot system with generalized coordinates ϕ, θ, x, y.

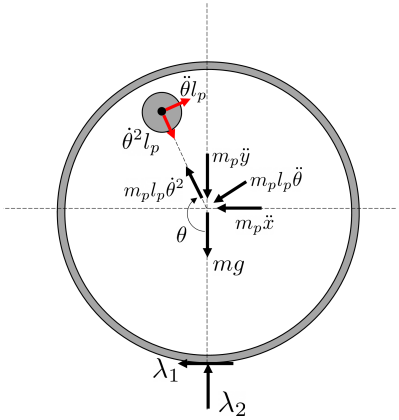

Fig. 3: Free body diagram of detached wheel, indicating the effects of the pendulum acceleration on the wheel.

Then, taking the Lagrangian as $\mathcal{L} = \mathcal{T} - \mathcal{V}$, we can write the equations of motion from the Euler-Lagrange equations:

$$\frac{d}{dt}\left(\frac{\partial \mathcal{L}}{\partial \dot{q}_i}\right) - \frac{\partial \mathcal{L}}{\partial q_i} = \sum_j \lambda_j \frac{\partial f_j^{\text{con}}}{\partial q_i} + f_i^{\text{ext}} \tag{4}$$

for $i = 1, \ldots, 4$ where f_j^{con} $(j = 1, 2)$ are the holonomic constraints acting on the system, λ_j are the constraint forces required to satisfy these constraints, and f_i^{ext} are the non-conservative generalized forces acting on the system. The holonomic constraints associated with this system are those of pure rolling and contact with the flat surface:

$$f_1^{\text{con}} = \phi R - x = 0 \tag{5a}$$

$$f_2^{\text{con}} = y = 0\,. \tag{5b}$$

The external generalized forces are those associated with the torque, τ, applied by the motor to the pendulum and the hoop. This yields the following Euler-Lagrange equations

$$I_o\ddot{\phi} = R\lambda_1 - \tau \tag{6a}$$

$$m_p l_p^2\ddot{\theta} - m_p l_p\left(\ddot{x}\cos\theta + \ddot{y}\sin\theta + g\sin\theta\right) = \tau \tag{6b}$$

$$m\ddot{x} + m_p l_p\left(\dot{\theta}^2\sin\theta - \ddot{\theta}\cos\theta\right) = -\lambda_1 \tag{6c}$$

$$m\ddot{y} + m_p l_p\left(\dot{\theta}^2\cos\theta + \ddot{\theta}\sin\theta\right) + mg = \lambda_2 \tag{6d}$$

where $m = m_o + m_p$ is the total mass of the hoop-pendulum system. Physically, λ_1 and λ_2 are the friction force required to maintain pure rolling and the normal force required for the body to remain in contact.

From the Newtonian perspective, Eqs. 6a-6b represent a sum of moments acting on the detached hoop and pendulum respectively, while Eqs. 6c-6d express the sum of forces acting on the pendulum-hoop system in the x and y directions, respectively. From Eq. 6d, it can be seen that when the angular velocity of the pendulum, $\dot{\theta}$ is large, the centripetal force due to the rotation of the pendulum will tend to have a lifting effect on the hoop when the pendulum is near the upright position, $\theta \approx \pi$. This effect is illustrated in Fig. 3 When this is the case, the normal reaction, λ_2, can go to zero and a loss of contact is possible, at which point the center of mass will behave like a projectile. If at this point the vertical component of the center of mass velocity is positive, then the hoop will undergo a flight phase, resulting in a jumping or hopping motion. If on the other hand, the vertical velocity of the center of mass is negative, the hoop will tend to slip or skid at the instant that the normal reaction vanishes but not jump.

A. Rolling phase

During the rolling phase of motion, the hoop remains in contact with the ground and rolls without slip. Therefore, Eqs. 6 can be reduced by substituting the rolling constraints (Eqs. 5). This gives the following reduced equations of motion, which are valid during the rolling phase.

$$(I_o + mR^2)\ddot{\phi} + m_p l_p R(-\ddot{\theta}\cos\theta + \dot{\theta}^2\sin\theta) = -\tau \tag{7a}$$

$$m_p l_p^2\ddot{\theta} + m_p l_p(-R\ddot{\phi}\cos\theta + g\sin\theta) = \tau \tag{7b}$$

The expressions for the friction, λ_1, required to prevent slipping and the normal reaction, λ_2, during rolling are given as follows.

$$\lambda_1 = m_p l_p\left(-\dot{\theta}^2\sin\theta + \ddot{\theta}\cos\theta\right) - mR\ddot{\phi} \tag{8a}$$

$$\lambda_2 = m_p l_p\left(\dot{\theta}^2\cos\theta + \ddot{\theta}\sin\theta\right) + mg \tag{8b}$$

As discussed above, the transition from a rolling phase to a flight phase occurs when the normal force vanishes and the velocity of the center of mass has a positive upward component. It is also possible for an intermediate phase to occur in which the friction provided by the rolling surface is insufficient to maintain the pure rolling constraint. In this case, the hoop could undergo slipping, skidding, or gliding motions [10], [28]. In this work, we will assume that such effects are negligible.

B. Flight phase

During the flight phase of motion, neither the contact nor rolling constraints are active, and thus the corresponding

constraint forces can be set to zero, $\lambda_1 = \lambda_2 = 0$, to give the following

$$I_o\ddot{\phi} = -\tau \tag{9a}$$

$$m_p l_p^2\ddot{\theta} - m_p l_p\left(\ddot{x}\cos\theta + \ddot{y}\sin\theta + g\sin\theta\right) = \tau \tag{9b}$$

$$m\ddot{x} + m_p l_p\left(\dot{\theta}^2\sin\theta - \ddot{\theta}\cos\theta\right) = 0 \tag{9c}$$

$$m\ddot{y} + m_p l_p\left(\dot{\theta}^2\cos\theta + \ddot{\theta}\sin\theta\right) + mg = 0 \tag{9d}$$

The center of mass of the system will undergo projectile motion during the flight phase, and thus will follow a parabolic trajectory, but this full system of equations is needed to describe the internal rotations of the system and the trajectory of the geometric center of the hoop.

IV. Control Strategy and Numerical Simulation

To numerically simulate this system, we implement the equations of motion described in Sec. III in MATLAB. To demonstrate the rolling, jumping motion, we consider the case where the robot begins at rest with the pendulum in the vertically downward position and the robot will be controlled using a proportional controller to choose the torque τ based on the error from a reference signal for the angular velocity of the pendulum relative to the wheel. We denote this angular velocity as $\dot{\psi} = \dot{\theta} - \dot{\phi}$. Such a simulation is shown in Fig. 4 and is explained in more detail in Sec. IV-C, but first we will discuss the control strategies implemented to achieve rolling and jumping motions.

A. Rolling strategy

To achieve a smooth rolling motion from rest, a torque should be applied to lift the pendulum toward the desired direction of motion. The resulting offset of the pendulum will cause the wheel to roll to restore the pendulum to the stable, downward equilibrium, thus leading the wheel to accelerate in the direction of the pendulum. Once the wheel is in rolling motion, it's velocity can be maintained by driving the pendulum so that it remains in the downward position. This is done by driving the pendulum so that its angular velocity relative to the wheel offsets the velocity of the wheel; that is, $\dot{\psi} = -\dot{\phi}$ so that $\dot{\theta} = 0$. This has the effect of holding the pendulum in the downward position in the spatial frame, but requires continuous actuation to move the pendulum relative to the rolling wheel. Following a similar reasoning, the wheel speed can be increased in a given direction by driving the pendulum relative to the wheel in such a way that the pendulum is displaced in that direction in the spatially fixed frame.

B. Jumping strategy

As mentioned previously in Sec. III, jumping motion will tend to occur when the pendulum has large angular velocity (relative to the spatially fixed frame) and the pendulum nears the upward configuration ($\theta \approx n\pi$ and $\dot{\theta}^2 \gg 1$), which causes the $m_p l_p \dot{\theta}^2 \cos\theta$ term in Eqs. 6d and 8b to become large, which leads the normal reaction λ_2 to vanish with the

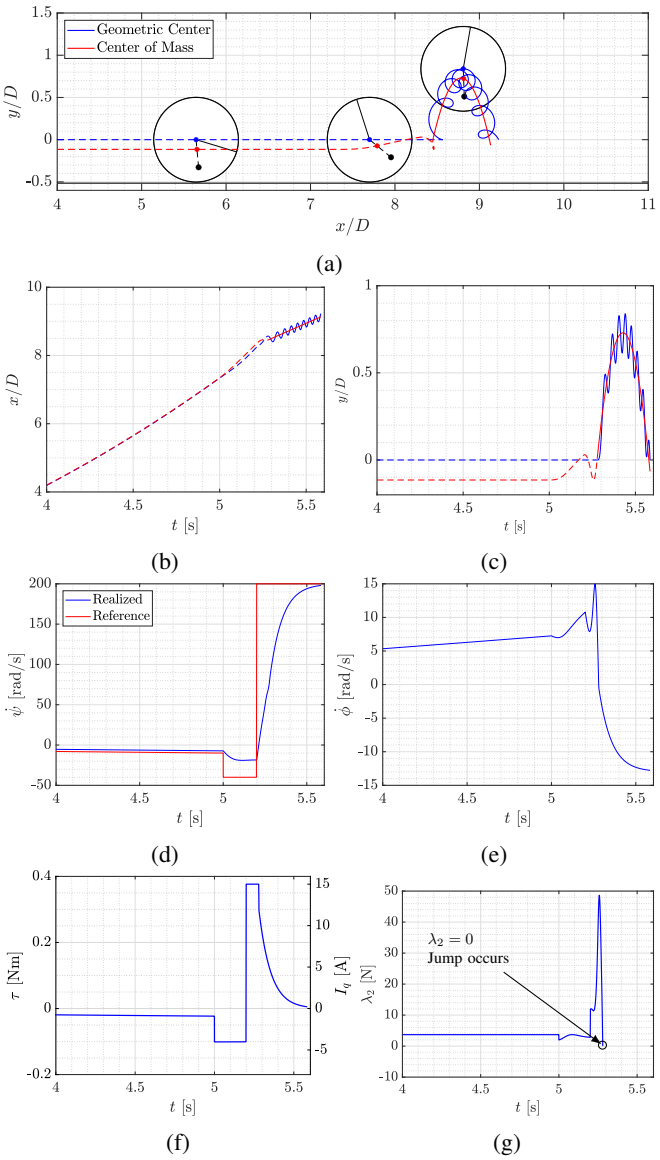

Fig. 4: Numerical simulation of the jumping wheel system. Dashed lines indicate the rolling phase while solid lines indicate the flight phase. (a) Spatial trajectory of the system center of mass and geometric center. (b)-(c) trajectories of these points over time. (d) relative angular velocity between the pendulum and the wheel (e) angular velocity of the wheel(f) torque values τ and corresponding motor currents I_q. (g) normal reaction λ_2 during rolling.

center of mass velocity having a positive vertical component. Therefore, to achieve a jump, the pendulum should be driven at high angular velocity toward the upward configuration once the desired rolling velocity is reached.

Increasing the horizontal distance traversed during the jump is a matter of increasing the horizontal component of the velocity of the center of mass at the instant that the loss of contact occurs, as from that point forward, the center of mass behaves as a projectile, and thus its displacement is a function of its initial position and velocity alone. The horizontal component of the center of mass velocity during rolling is

$\dot{\phi}R - \frac{m_p l_p}{m_o+m_p}\dot{\theta}\cos\theta$. So, the horizontal displacement can be increased by increasing the rolling speed of the wheel, $\dot{\phi}R$. However, this can be a difficult balance due to actuator limits, as a higher rolling speed means that there will be less time for the pendulum to accelerate from its downward position during rolling to the upward configuration necessary for a jump. Therefore, in practice, we have found that better jumping can be achieved by first initiating a slow "swing-up" phase in which the pendulum is brought to the upward position at a low enough angular velocity so that a loss of contact is not realized before actuating the pendulum with maximum torque in the opposite direction so that the pendulum has the time taken to traverse the full revolution back to the upward position to accelerate and maximize $\dot{\theta}^2$.

C. Numerical simulation

As proof of concept, we implement a numerical simulation of the proposed control strategy. In this simulation, the wheel is started from rest with the pendulum in the vertically downward position. The torque is chosen by applying a proportional controller relative to a reference relative angular velocity, $\dot{\psi}_{\text{ref}}$. This reference angular velocity is chosen to give a 5s rolling period in which the wheel accelerates from rest to an angular velocity of approximately 10 rad/s, causing the wheel to roll from left to right. For this, the reference angular velocity is chosen to be linear in time. Following this rolling phase, the swingup-phase is initiated, in which the pendulum is brought counterclockwise to the upward position at an angular velocity slow enough so that loss of contact does not occur. Finally, the pendulum is actuated clockwise at a large angular velocity in order to achieve a jump as the pendulum nears the upward configuration. In summary, the relative angular velocity reference command is chosen as follows:

$$\dot{\psi}_{\text{ref}}(t) = \begin{cases} -2t & t < 5 \\ -40 & 5.0 < t < 5.2 \\ 200 & t > 5.2 \end{cases} \tag{10}$$

where the times are given in seconds and the angular velocities are in rad/s. All parameters used in this simulation are selected to be representative of the robot described in Sec II.

The simulation is conducted by first simulating the rolling dynamics given by Eqs. 7. These equations are simulated until a point is reached where the normal reaction vanishes and the vertical velocity of the center of mass is upward, at which point this terminal condition of the rolling phase is taken as the initial condition for the flight phase and the system is simulated from there using the flight dynamics given by Eqs. 9. The results of this simulation are shown in Fig. 4. Figs. 4a-4c show the trajectory taken by the robot in this simulation in xy space and over time, respectively. It can be seen from these figures that while in the air, the center of the hoop follows a cycloidal trajectory, revolving about the trajectory of the center of mass, which follows a parabolic trajectory. These revolutions of the wheel center about the center of mass are due to the driving of the pendulum relative to the wheel. The simulation is ended when the y coordinate of the center of the wheel returns to zero, indicating that the wheel has landed on the ground. To continue the simulation from there, it would be necessary to account for the collision dynamics associated with the impact with the ground.

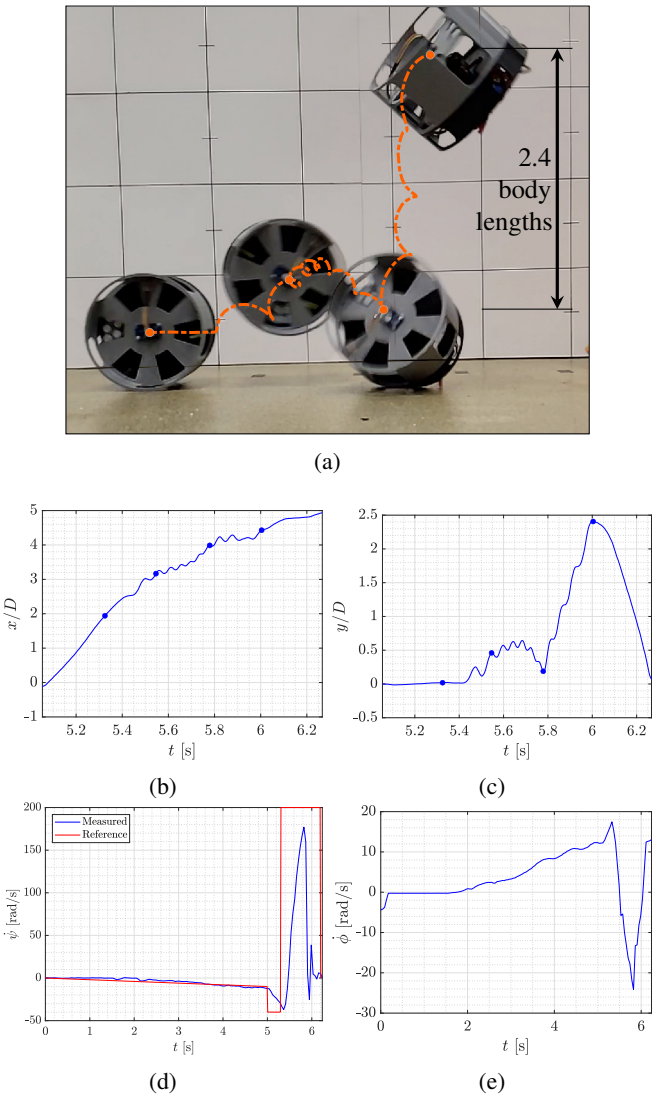

Fig. 5: Experimental results for vertical jumping. (a) Four still images from a video of the jumping motion overlaid to illustrate the robot trajectory. (b)-(c) Trajectory of a point on the front of the wheel over time. (d) Relative angular velocity between pendulum and wheel. (e) Angular velocity of the wheel.

V. Experimental Results

A. Jumping experiment

Following the results of the numerical experiment described in the previous section, the same experiment is conducted on the robot described in Sec. II. In this experiment, the same reference velocity is provided to the motor as given by Eq. 10. The result of this experiment is shown in Fig. 5. Video of the experiment was recorded at 240 frames/second

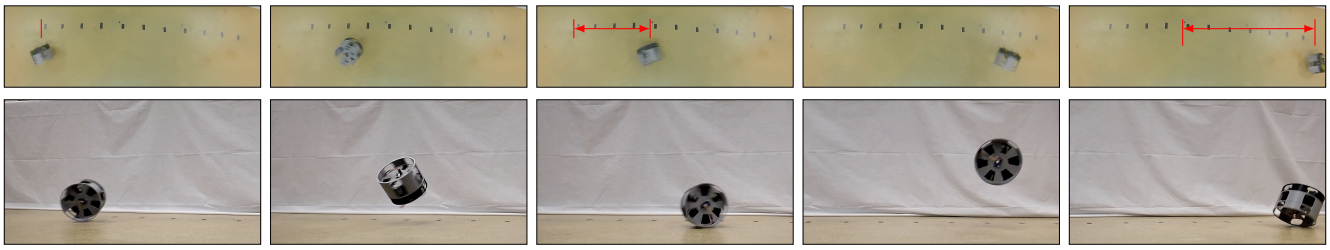

(a) (b) (c) (d) (e)

Fig. 6: Jumping while traversing a horizontal distance.
Top row: a sequence of frames from an overhead camera. Black floor markings indicate distances of one body length. Red lines indicate the landing positions of the robot and the distances traversed between them. The distance indicated in panel (c) is approximately 4 body lengths and the distance indicated in panel (e) is approximately 6 body lengths.
Bottom row: corresponding images from the same sequence, taken from a side view panning along with the robot.

(fps) from a side view with a stationary camera. Fig. 5a shows four frames from this recording overlaid with one another to represent the path followed by the robot during the jump. The video was post-processed using the software, Tracker (https://physlets.org/tracker/) to obtain the trajectory followed by a point located on the center of the front hoop. This trajectory is given by the curve plotted over the image and is shown over time in Figs. 5b, 5c. The four points on the trajectory that are overlaid in Fig. 5a are indicated the plots in Fig. 5b, 5c by the blue circles. It can be seen from this trajectory that the motion of the robot agrees with the numerical simulation of the previous section. The robot completes a small hop followed by a small jump and then a large jump. The simulation of the previous section predicts the small jump height well, both showing this height to be approximately 0.7-0.8 body lengths. In the experiment, following this first jump, the robot rebounds into a section jump, achieving a height of approximately 2.4 body lengths, as shown in Fig. 5a. Fig. 5d shows the relative angular velocity of the pendulum to the hoop during the experiment as measured from the onboard encoder along with the corresponding reference signal in Eq. 10. Fig. 5e shows the wheel angular velocity as measured from the onboard IMU.

B. Horizontal jumping

In an additional experiment, we apply a different reference angular velocity in an attempt to clear a larger horizontal distance during the jump. In particular, we attempt to have the robot reach a larger horizontal velocity before initiating the jump. This is done by driving the pendulum so that the angular velocity of the wheel increases more rapidly, accelerating from rest to an angular velocity of approximately 23 rad/s over 3.75s. At this point, the jump is initiated by applying an angular velocity reference of 150 rad/s in the same direction as the rotation of the pendulum for jumping. This reference signal is summarized as follows.

$$\dot{\psi}_{\text{ref}}(t) = \begin{cases} -6.22t & t < 3.75 \\ -150 & 3.75 < t < 4.75 \end{cases} \tag{11}$$

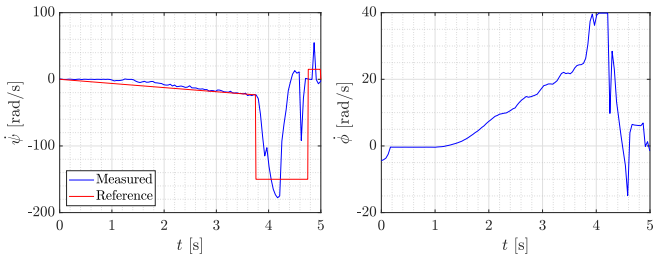

(a) (b)

Fig. 7: Measured data from horizontal jumping experiment shown in Fig. 6. (a) Relative angular velocity between pendulum and wheel. (b) Angular velocity of the wheel.

The direction of rotation for initiating the jump for this test was chosen to be the same direction as the rolling direction because it was seen in previous experiments (including the experiment of Fig. 5) that by initiating the jump by swinging the pendulum counter to the direction needed for rolling, while leading to a larger vertical height of the jump, can have a braking effect on the rolling motion, leading to a reduced horizontal velocity of the center of mass at the loss of contact, and therefore a reduced horizontal distance traversed while in flight.

Results from this test are shown in Fig. 6. The trial was recorded at 240 fps from a side view taken from a panning camera and additionally from a stationary camera mounted overhead, recording at 120 fps. Five still images from each of these views are aligned and shown in Fig. 6. The top row of Fig. 6 shows views from the overhead camera, where the black markings on the ground are evenly spaced ticks with spacings of one diameter separating each.

During this experiment, once the jump is initiated, the robot completes one small hop, followed by two jumps in which a significant horizontal distance is cleared. The red marking in the top panel of Fig. 6a indicates the landing position after the first small hop. Fig. 6b shows the robot in mid-flight after launching from the position shown in Fig. 6a. Fig. 6c shows the landing position of the robot following the first significant jump. The top panel of Fig. 6c shows

a red marking indicating the landing position along with a line indicating the distance traversed during this first jump, which spans approximately 4 body lengths. Fig. 6d shows the robot in mid-flight after launching from the position shown in Fig. 6c . Finally, Fig. 6e shows the landing position of the robot during the second jump, with the top panel indicating the distance traversed during this jump, a horizontal span of over 6 body lengths. Fig. 7 shows the measured data collected in this experiment from the onboard encoder and IMU, respectively, along with the reference signal for the relative angular velocity in Eq. 11.

VI. Conclusion

We have presented a novel design for a pendulum-driven wheel robot that can both roll and jump. In experiments, the robot was capable of jumping up to 2.4 body lengths vertically and, in separate tests, was able to traverse horizontal lengths of over 6 body lengths in flight. Ongoing and future work on this robot include the development and implementation of trajectory planning and model-based control strategies, consideration of the full dynamics including 3D rotations and collision effects, designs and control strategies to allow for stabilization following a jump.

References

[1] J. Zhao, J. Xu, B. Gao, F. Cintron, M. Mutka, and L. Xiao, "Msu jumper: A single-motor-actuated miniature steerable jumping robot," *IEEE Transactions on Robotics*, vol. 29, no. 3, pp. 602–614, 2013.

[2] A. De and D. Koditschek, "Parallel composition of templates for tail-energized planar hopping," in *IEEE International Conference on Robotics and Automation*, pp. 4562–4569, 2015.

[3] U. Scarfogliero, C. Stefanini, and P. Dario, "Design and development of the long-jumping "grillo" minirobot," in *IEEE International Conference on Robotics and Automation*, pp. 467–472, 2007.

[4] D. W. Haldane, M. M. Plecnik, J. K. Yim, and R. S. Fearing, "Robotic vertical jumping agility via series-elastic power modulation," *Science Robotics*, vol. 1, no. 1, 2008.

[5] V. Zaytsev, U. B. Hanan, A. Weiss, G. Kósa, and A. Ayali, "A locust-inspired miniature jumping robot," *Bioinspiration and Biomimetics*, vol. 10, no. 6, 2015.

[6] J. Littlewood, *A Mathematicians Miscellany*. London: Methuen & Co. Ltd, 1953.

[7] T. F. Tokieda, "The Hopping Hoop," *The American Mathematical Monthly*, vol. 104, pp. 152–154, Feb. 1997.

[8] B. M. Shimomura Y and M. H.K, "Dynamics of an axisymmetric body spinning on a horizontal surface. ii. self-induced jumping," *Proceedings of the Royal Society A*, vol. 461, p. 1753–1774, 2005.

[9] A. Ivanov, "On detachment conditions in the problem on the motion of a rigid body on a rough plane," *Regular and Chaotic Dynamics*, vol. 13, p. 355–368, 2008.

[10] A. Bronars and O. M. O'Reilly, "Gliding motions of a rigid body: the curious dynamics of Littlewood's rolling hoop," *Proceedings of the Royal Society A: Mathematical, Physical and Engineering Sciences*, vol. 475, p. 20190440, Nov. 2019.

[11] P. Tallapragada, J. Buzhardt, and R. Seney, "A Passive Jumping Mechanism," (Park City, Utah, USA), p. V003T17A010, American Society of Mechanical Engineers, Oct. 2019.

[12] T. McGeer *et al.*, "Passive dynamic walking," *Int. J. Robotics Res.*, vol. 9, no. 2, pp. 62–82, 1990.

[13] M. Garcia, A. Chatterjee, A. Ruina, and M. Coleman, "The simplest walking model: stability, complexity, and scaling," 1998.

[14] S. Collins, A. Ruina, R. Tedrake, and M. Wisse, "Efficient bipedal robots based on passive-dynamic walkers," *Science*, vol. 307, no. 5712, pp. 1082–1085, 2005.

[15] R. Armour, K. Paskins, A. Bowyer, J. Vincent, and W. Megill, "Jumping robots: a biomimetic solution to locomotion across rough terrain," *Bioinspiration & biomimetics*, vol. 2, no. 3, p. S65, 2007.

[16] Y. Matsuyama and S. Hirai, "Analysis of circular robot jumping by body deformation," in *Proceedings 2007 IEEE International Conference on Robotics and Automation*, pp. 1968–1973, 2007.

[17] K. Misu, A. Yoshii, and H. Mochiyama, "A Compact Wheeled Robot that Can Jump while Rolling," in *2018 IEEE/RSJ International Conference on Intelligent Robots and Systems (IROS)*, (Madrid), pp. 7507–7512, IEEE, Oct. 2018.

[18] R. Hayashi and S. Tsujio, "High-performance jumping movements by pendulum-type jumping machines," in *Proceedings 2001 IEEE/RSJ International Conference on Intelligent Robots and Systems. Expanding the Societal Role of Robotics in the the Next Millennium (Cat. No.01CH37180)*, vol. 2, (Maui, HI, USA), pp. 722–727, IEEE, 2001.

[19] B. J. Hockman, A. Frick, R. G. Reid, I. A. Nesnas, and M. Pavone, "Design, control, and experimentation of internally-actuated rovers for the exploration of low-gravity planetary bodies," *Journal of Field Robotics*, vol. 34, no. 1, pp. 5–24, 2017.

[20] T.-M. Ho, V. Baturkin, C. Grimm, J. T. Grundmann, C. Hobbie, E. Ksenik, C. Lange, K. Sasaki, M. Schlotterer, M. Talapina, *et al.*, "Mascot—the mobile asteroid surface scout onboard the hayabusa2 mission," *Space Science Reviews*, vol. 208, pp. 339–374, 2017.

[21] A. R. Geist, J. Fiene, N. Tashiro, Z. Jia, and S. Trimpe, "The Wheelbot: A Jumping Reaction Wheel Unicycle," *IEEE Robotics and Automation Letters*, vol. 7, pp. 9683–9690, Oct. 2022.

[22] J. W. Romanishin, K. Gilpin, S. Claici, and D. Rus, "3d m-blocks: Self-reconfiguring robots capable of locomotion via pivoting in three dimensions," in *2015 IEEE International Conference on Robotics and Automation (ICRA)*, pp. 1925–1932, IEEE, 2015.

[23] M. Muehlebach and R. D'Andrea, "Nonlinear analysis and control of a reaction-wheel-based 3-d inverted pendulum," *IEEE Transactions on Control Systems Technology*, vol. 25, no. 1, pp. 235–246, 2016.

[24] E. Kayacan, Z. Y. Bayraktaroglu, and W. Saeys, "Modeling and control of a spherical rolling robot: a decoupled dynamics approach," *Robotica*, vol. 30, no. 4, pp. 671–680, 2012.

[25] G. W. Howell, *Analysis and control of superarticulated biped robots*. PhD thesis, 2000.

[26] P. A. Bhounsule, E. Ameperosa, S. Miller, K. Seay, and R. Ulep, "Dead-Beat Control of Walking for a Torso-Actuated Rimless Wheel Using an Event-Based, Discrete, Linear Controller," in *Volume 5A: 40th Mechanisms and Robotics Conference*, (Charlotte, North Carolina, USA), p. V05AT07A042, American Society of Mechanical Engineers, Aug. 2016.

[27] S. Sanchez and P. A. Bhounsule, "A differential drive rimless wheel that can move straight and turn," in *2020 IEEE/ASME International Conference on Advanced Intelligent Mechatronics (AIM)*, (Boston, MA, USA), pp. 514–519, IEEE, July 2020.

[28] A. Taylor and M. Fehrs, "The dynamics of an eccentrically loaded hoop," *American Journal of Physics*, vol. 78, pp. 496–498, May 2010.